Journal of Power Sources 366 (2017) 80–85

Contents lists available at ScienceDirect

Journal of Power Sources

journal homepage: www.elsevier.com/locate/jpowsour

# *In situ* measurement of mechanical property and stress evolution in a composite silicon electrode

Dawei Li [a, b], Yikai Wang [b], Jiazhi Hu [b], Bo Lu [a], Yang-Tse Cheng [b], Junqian Zhang [c, d, e, *]

[a] Shanghai Institute of Applied Mathematics and Mechanics, Shanghai University, Shanghai 200072, China
[b] Department of Chemical and Materials Engineering, University of Kentucky, Lexington, KY 40506, USA
[c] Department of Mechanics, Shanghai University, Shanghai 200444, China
[d] Shanghai Key Laboratory of Mechanics in Energy Engineering, Shanghai 200072, China
[e] Materials Genome Institute, Shanghai University, Shanghai 200444, China

## HIGHLIGHTS

- Large curvature change of a Si/PVDF composite electrode is observed during cycling.
- A method is proposed to measure elastic modulus and stress in the electrode.
- Effect of crack formation on stress evolution and mechanical behavior is revealed.

## ARTICLE INFO

*Article history:*
Received 3 June 2017
Received in revised form
1 August 2017
Accepted 1 September 2017

*Keywords:*
Lithium-ion battery
Silicon composite electrode
*In situ* measurement
Fracture
Modulus
Diffusion induced stress

## ABSTRACT

Mechanical properties and lithiation-induced stress are crucial to the performance and durability of lithium-ion batteries. Here, we report the evolution of elastic modulus and stress in a silicon/polyvinylidene fluoride (PVDF) composite electrode coated on a copper foil, along with a model for analyzing the large change in the radius of curvature of the composite electrode/copper foil cantilever. The radius of curvature of the cantilever is captured by a video camera during lithiation/delithiation. The elastic modulus of the composite electrode decreases from about 0.64 GPa to 0.18 GPa during lithiation. It decreases further to about 0.10 GPa after delithiation, which is caused by the fracture of the electrode. The magnitude of the compressive stress increases lineally during lithiation and decreases suddenly to reach a steady state value during delithiation.



## 1. Introduction

Stress effects on the performance and durability of lithium-ion batteries (LIBs) have been widely investigated [1–3] to help develop the next generation of LIBs with higher energy density, longer cycle life, and faster rate capabilities. Specifically, silicon (Si) is one of the most promising negative electrode materials because of its high theoretical capacity (~3600 $mAhg^{-1}$). However, compared with commercially used graphite electrodes, Si experiences much larger volumetric expansion upon fully lithiation (~12% for graphite; 300% for Si) which can cause significant stress [4], leading to cracking and delamination. Hence, observing stress evolution and measuring changes in mechanical properties of Si-based electrodes during electrochemical cycling are crucial for understanding and enabling these electrodes for future LIB applications.

Several *in situ* measurements of the changes in structure, composition, and morphology of the electrodes have been reported in the literature, including transmission electron microscopy [5], x-ray transmission microscopy [6], atomic-force microscopy (AFM) [7,8], nuclear magnetic resonance (NMR) [9] and optical stress sensors. Usually, *in situ* measurements were conducted in thin film electrodes. For example, Dahn and co-workers [10,11] used *in situ* optical microscopy and AFM to study deformation in Li-alloy thin film electrodes and revealed that cracks appeared primarily due to

* Corresponding author. Department of Mechanics, Shanghai University, Shanghai 200444, China.
*E-mail addresses:* lidawei.134@163.com (D. Li), yang.t.cheng@uky.edu (Y.-T. Cheng), jqzhang2@shu.edu.cn (J. Zhang).

http://dx.doi.org/10.1016/j.jpowsour.2017.09.004
0378-7753/

the lateral contraction of the films during the delithiation process. Stress evolution of thin film electrodes has been monitored by the *in situ* wafer-curvature technique [12–16]. It measures the change in the curvature of the inactive and stiff substrate and then converted it to an in-plane stress in the film using Stoney's equation [17]. In additional to measuring stress, Sethuraman et al. [13–15] completed a series of wafer-curvature experiments to monitor the changes in thin film electrode properties, such as biaxial modulus and stress-potential coupling, during electrochemical cycling. The same technique was also used to obtain real-time stress measurements on carbon thin film electrodes and the stress at the substrate/current collector was about 0.25 GPa [12]. These studies provide insights into the mechanisms associated with deformation and stress development in LIB electrodes.

The mechanical properties of LIB electrodes have also been calculated by *ab initio* quantum mechanics. Qi et al. [18] studied the Young's modulus of graphite electrodes during lithium intercalation using the Density Functional Theory and found that the polycrystalline Young's modulus of graphite electrode tripled as it was lithiated to $LiC_6$. Yang et al. [19] calculated that the Young's modulus of $Li_xSi$ would decrease from 160 to 40 GPa with increasing Li content in the alloy. However, the *in situ* experimental measurement of mechanical properties such as elastic modulus is much needed.

Composite electrodes, which are typical in commercial LIBs, have a complex porous structure consisting of active particles, conductive graphite, and polymeric binders. It is difficult to measure *in situ* mechanical properties and stress evolution in composite electrodes during electrochemical cycling. The objective of this work is to measure *in situ* the elastic modulus and stress evolution in a composite Si/PVDF electrode. A cell made of quartz was constructed for *in situ* measurements of the curvature change of the composite electrode and a mathematical model was developed to analyze the evolution of curvature, modulus, and stress in the composite electrode during electrochemical cycling.

## 2. Experiment

### 2.1. Electrode preparation and cell assembly

Composite Si electrodes were made by mixing 50 wt% Si powder (size 30–50 nm, Nanostructured & Amorphous Materials), 25 wt% conductive carbon black (Super P C65, TIMCAL), and 25 wt% PVDF binder (Alfa Aesar) to form a slurry [20]. The N-methyl-2-pyrrolidone (NMP, 99.5%, Alfa Aesar) was used as the solvent to dissolve PVDF (weight ratio of 36.3:1). Then, the slurry was casted onto a battery grade Cu foil (24 μm thick) by using a 127 μm gap doctor blade. The electrodes were dried at 130 °C for 12 h in a vacuum oven. A calendering machine (MIT Corporation) was used to press the electrode to a porosity of 32.5% (see Table 1 and Appendix).

A layered electrode configuration shown in Fig. 1 was used to investigate the relationship between curvature ($\kappa$) and the state of charge (SOC) in the electrochemical experiments. The electrochemical cell is made of transparent quartz which allows the measurement of the deformation of the layered electrode by a video camera (JAI). A porous 12 μm thick Si/PVDF composite electrode deposited on a 24 μm thick copper foil served as the working electrode, while a lithium metal (3 mm thick, 60 mm length and 4 mm width, Sigma Aldrich) was used as both a reference and counter electrode. The two electrodes, in the form of two cantilever beams, were positioned facing each other and separated by a piece of microporous polypropylene film (Woven Celgard C3501 separator of thickness 21 μm, Celgard, Inc.). The cell was filled with 1 M $LiPF_6$ salt in a mixture of ethylene carbonate and diethyl carbonate (EC: DEC = 1:1 vol%, BASF). The experiment was done in a glove-box filled with ultra-high purity argon.

**Table 1**
The volume fraction of each composition.

| | Mass (mg) | Density (g/cm$^3$) | Volume (cm$^3$) | Volume fraction |
|---|---|---|---|---|
| Si | 0.8920.357 | 2.329 | 0.000153 | 28.3% |
| CB | 0.1785 | 1.6 | 0.000112 | 20.5% |
| PVDF | 0.1785 | 1.77 | 0.000101 | 18.7% |
| Porosity | – | – | – | 32.5% |

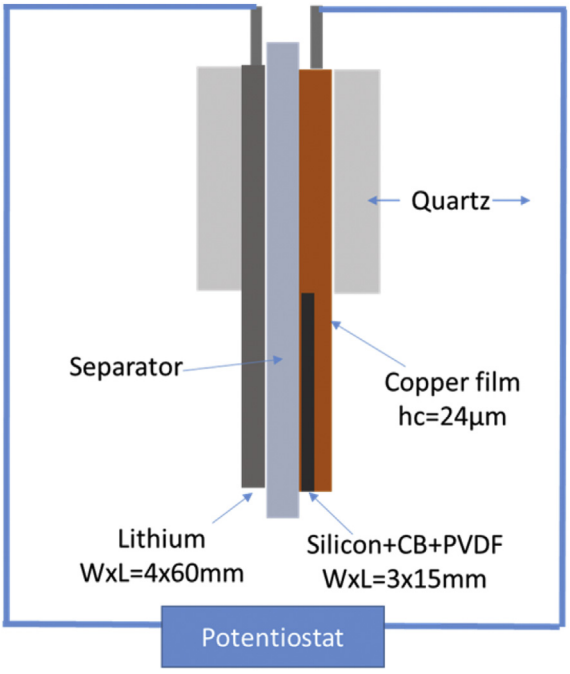


**Fig. 1.** A schematic illustration of the electrochemical cell.

### 2.2. Electrochemical test

Electrochemical cycling of the composite Si electrode was carried out in the cell described above at room temperature using Bio-Logic potentiostats (MPG-2 and VMP-3, BioLogic). The cell was cycled galvanostatically at a current density of 142.1 μA/cm$^2$ (ca.$C$/20C-rate, theoretical capacity of 3600 mAhg$^{-1}$ for silicon) for 6 h, followed by an open-circuit potential relaxation for 4 min between 0.01 and 2V *vs*. Li/Li$^+$. A charge-coupled video camera (JAI) was used to acquire pictures of the electrode during electrochemical cycling. Fig. 2 shows the change in the curvature of the composite electrode during lithiation.

### 2.3. Mathematical model of curvature change

Mechanical analysis provides an insight into the mechanism of deformation process. Fig. 3a illustrates the bilayer electrode geometry in the experiments by bonding an active layer to a current collector to form a cantilever. Here, $h_1$ and $h_c$ denote the thickness of the active layer and current collector, respectively. The composite electrode expands and contracts as lithium diffuses into and out of the active layer during electrochemical cycling. As the active layer expands (contracts) while the current collector restricts it, the composite electrode will bend to a larger (smaller) curvature, as shown in Fig. 3b. Let the thickness direction be aligned with the $z$-axis and the plate is in the $x$-$y$ plane. Lithium ions are allowed to be

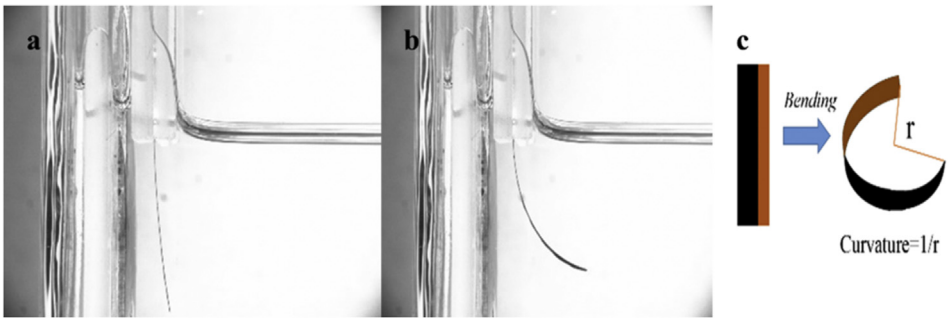


**Fig. 2.** Photographs of a composite-electrode (a) before and (b) during experiments; (c) schematic of the curvature of the electrode.

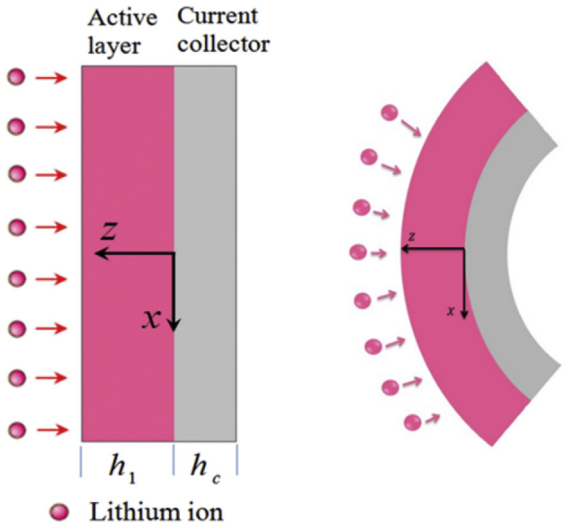


**Fig. 3.** Configuration of the electrode in which an active layer is bonded to the current collector.

inserted into and extracted out of the electrode from outside of active material layer, as shown in Fig. 3.

Under the elastic deformation theory [3,21], the in-plane normal strain has a liner variation in the thickness direction, and can be written as:

$$\varepsilon = \varepsilon_0 + \kappa z \tag{1}$$

where $\varepsilon_0$ is the in-plane strain at the plane of $z = 0$ characterizing the elongation strain of the electrode, and $\kappa$ is curvature. This equation implies that the active layer and current collector are bonded well and have the same bending curvature.

Although the active layer is a composite consisting of active particles, polymeric binder, conducting agent, and porosity, we assume that it is macroscopically homogeneous, isotropic, and elastic. When the electrode is cycled at a relatively slow charge and discharge rate, the concentration $c$ can be assumed to be a constant along the z-axis. The constitutive equation of the active layer can be expressed as:

$$\begin{aligned} \sigma_1 &= E_1(c)(\varepsilon_0 + z\kappa) - \frac{1}{3}E_1(c)\Omega c \\ \sigma_c &= E_c(\varepsilon_0 + z\kappa) \end{aligned} \tag{2}$$

where $E_1(c)$ is the Young's modulus of the electrode which is a function of the Li concentration, and $\Omega$ is partial molar volume of active layer. The concentration dependent term $-E\Omega c/3$ represents the diffusion induced stress in the active layer.

Assuming that the bilayer is free of any mechanical constraint and the total force and toque balances require:

$$\int_{-h_c}^{h_1} \sigma_x dz = 0 \qquad \int_{-h_c}^{h_1} \sigma_x z dz = 0 \tag{3}$$

Substituting Eq. (2) into Eq. (3), yields the strain $\varepsilon_0$ and curvature $\kappa$ of the electrode as:

$$\kappa = \frac{\Omega}{3h_1^3}\frac{\alpha_1}{\alpha}\int_0^{h_1} czdz + \frac{\Omega}{3h_1^2}\frac{\alpha_2}{\alpha}\int_0^{h_1} cdz = \frac{2\alpha_5\Omega c}{h_1\alpha} \tag{4}$$

$$\varepsilon_0 = \frac{\Omega}{3h_1^2}\frac{\alpha_2}{\alpha}\int_0^{h_1} czdz + \frac{\Omega}{3h_1}\frac{\alpha_3}{\alpha}\int_0^{h_1} cdz = \frac{\alpha_4\Omega c}{3\alpha} \tag{5}$$

where

$$\alpha_1 = 12\left(1 + \frac{E_c}{E_1}\frac{h_c}{h_1}\right), \alpha_2 = 6\left(-1 + \frac{E_c}{E_1}\left(\frac{h_c}{h_1}\right)^2\right)$$

$$\alpha_3 = 4\left(1 + \frac{E_c}{E_1}\left(\frac{h_c}{h_1}\right)^3\right), \alpha_4 = 1 + 3\frac{E_c}{E_1}\left(\frac{h_c}{h_1}\right)^2 + 4\frac{E_c}{E_1}\left(\frac{h_c}{h_1}\right)^3, \alpha_5 = \frac{E_c}{E_1}\frac{h_c}{h_1} + \frac{E_c}{E_1}\left(\frac{h_c}{h_1}\right)^2$$

$$\alpha = \left(1 + 4\frac{E_c}{E_1}\frac{h_c}{h_1} + 6\frac{E_c}{E_1}\left(\frac{h_c}{h_1}\right)^2 + 4\frac{E_c}{E_1}\left(\frac{h_c}{h_1}\right)^3 + \left(\frac{E_c}{E_1}\right)^2\left(\frac{h_c}{h_1}\right)^4\right) \tag{6a-f}$$

Here, $\alpha$-$\alpha_5$ depend on sample configuration, e.g., electrode thickness $h_1$ and copper foil thickness $h_c$, and elastic modulus of the electrode $E_1$ and copper foil $E_c$. Rewriting Eq. (4), we obtain a quadratic equation of the curvature and modulus ratio $R_E = E_c/E_1$, thickness ratio $R_h = h_c/h_1$ and Li concentration $c$. This equation and its solution are given in Eqs. (7) and (8):

$$\kappa h_1 R_h^4 R_E^2 + \left(4\kappa h_1 R_h + 6\kappa h_1 R_h^2 + 4\kappa h_1 R_h^3 - 2\Omega c R_h - 2\Omega c R_h^2\right)R_E + \kappa h_1 = 0 \tag{7}$$

$$R_E = \frac{\left( -\left(4\kappa h_1 R_h + 6\kappa h_1 R_h^2 + 4\kappa h_1 R_h^3 - 2\Omega c R_h - 2\Omega c R_h^2\right) + \sqrt{\left(4\kappa h_1 R_h + 6\kappa h_1 R_h^2 + 4\kappa h_1 R_h^3 - 2\Omega c R_h - 2\Omega c R_h^2\right)^2 - 4\kappa^2 h_1^2 R_h^4} \right)}{2\kappa h_1 R_h^4} \quad (8)$$

The elastic modulus evolution with Li concentration in the Si composite electrode can be calculated by monitoring the curvature change *vs.* time of the electrode using the CCD camera and by measuring the thickness parameters $h_c$ and $h_1$ with a micrometer (Mitutobo). Also, the in-plain strain, $\varepsilon_0$, is a function of $R_E$,$R_E$ and Li concentration $c$, as shown in Eq. (5). Stress measurements during electrochemical cycling of the composite electrode can be performed by combining Eqs. (2), (4) and (5).

Based on the photos collected by the video camera, we can extract the deformation data using a getdata graph digitizer to obtain the curvature as a function of lithiation and delithiation (Fig. 2c).

## 3. Results and discussion

Fig. 4 shows cell potential and deformation of the Si/PVDF composite electrode plotted against time in the first 3 cycles. The composite electrode undergoes large deformation during lithiation/delithiation cycles. Upon lithiation, Li-ions continuously react with Si and cause the active layer to expand while the current collector restricts its expansion. The mismatch deformation bends the electrode. With increasing SOC, the deformation of the active layer increases gradually, resulting in a large curvature. The delithiation process reverses the change in the curvature of the electrode. The deformation in the first cycle is smaller than with subsequent cycles due to solid-electrolyte interphase (SEI) formation [22], which consumes a considerable amount of Li-ions. As a result, fewer lithium ions would react with Si in the first cycle, leading to smaller deformation. With increasing number of cycles, the deformation causes cracks in the electrode (to be discussed more in detail later in this section). As a result, the maximum curvature in the 3rd cycle is, as shown in Fig. 4, smaller than that in the 2nd cycle. We focus on the curvature change in the second cycle.

Fig. 5 shows the thickness evolution of the electrode measured with a micrometer (Mitutobo). The thickness increases in the lithiation process and decreases in the delithiation process approximately linearly with $h = 44 + 0.45 \times SOC$ in the lithiation process and $h = 39.5 + 0.61 \times SOC$ in the delithation process, respectively. Cracks form with the SOC during lithiation and, more prominently during delithiation, as shown in Fig. 6.

Now we use the Eq. (8) along with the curvature data given in Fig. 4 to extract the elastic modulus of composite electrode. In order to do so the partial molar volume of silicon is assumed to be constant $\Omega_{Si} = 8.25 \times 10^{-6} mol/m^3$ [23], $\Omega_{Si} c_{\max}$ is the volumetric strain at full lithiation, which is about 300% volume expansion for silicon. Volume expansion of composite electrode is believed to be smaller than expansion of silicon since the other compositions do not change in volume and the porosity could accommodate some volume expansion of silicon. Hence it is assumed that the volume expansion of composite electrode is proportional to the volume expansion of silicon by the silicon volume fraction (28.3% estimated for our composite electrode, see appendix), *i.e.* $\Omega_{composites} c = \Omega_{Si} c_{max} \times SOC \times 0.283$. Substituting the curvature *vs.* Li concentration and thickness ratio $R_h = h_c/h_1$, elastic modulus of current collector $E_c = 117$ GPa [24] into Eq. (8), the elastic modulus of composites electrode *vs.* Li concentration is obtained, as shown in Fig. 7. The measured modulus of the composite is an average value of the whole composite electrode, including the coupling effect of porosity and volume expansion. This method has considered the effect of extensional stiffness, stretching-bending coupling stiffness, bending stiffness [3] of current collector on the extraction of elastic modulus in the lithiation/delithiation process.

The results show that the Si composite electrode softens significantly, decreasing from an initial modulus value of 0.64 GPa–0.18 GPa when the capacity is 1080 mAhg$^{-1}$ during the

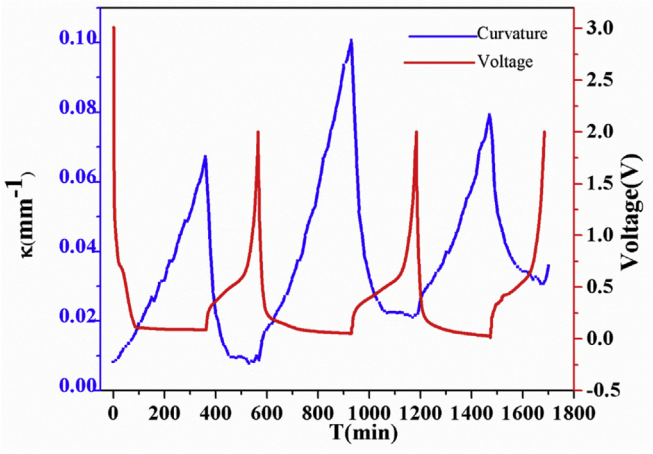


**Fig. 4.** Potential and curvature profiles of the Si/PVDF composite electrode during the first 3 lithiation/delithiation cycles are shown against the time. The electrode was galvanostatically cycled at a current density of 142.1 μA/cm$^2$ (ca. C/20) with a lower and upper cutoff of 0.01–2 V *vs.* Li/Li$^+$, respectively.

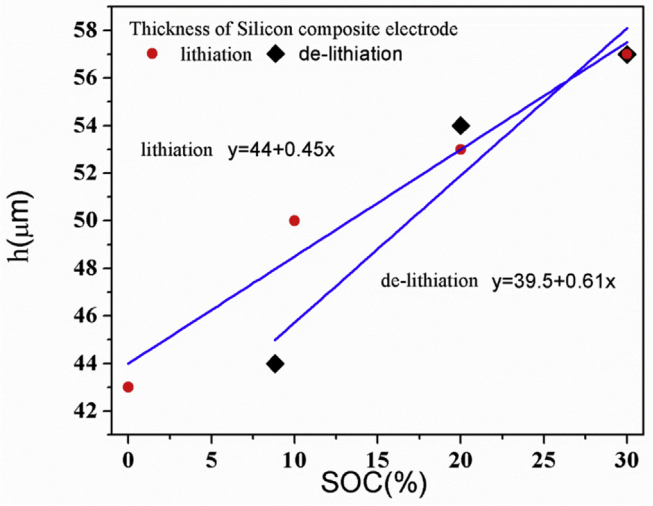


**Fig. 5.** Thickness evolution of the electrode in 2nd cycle.

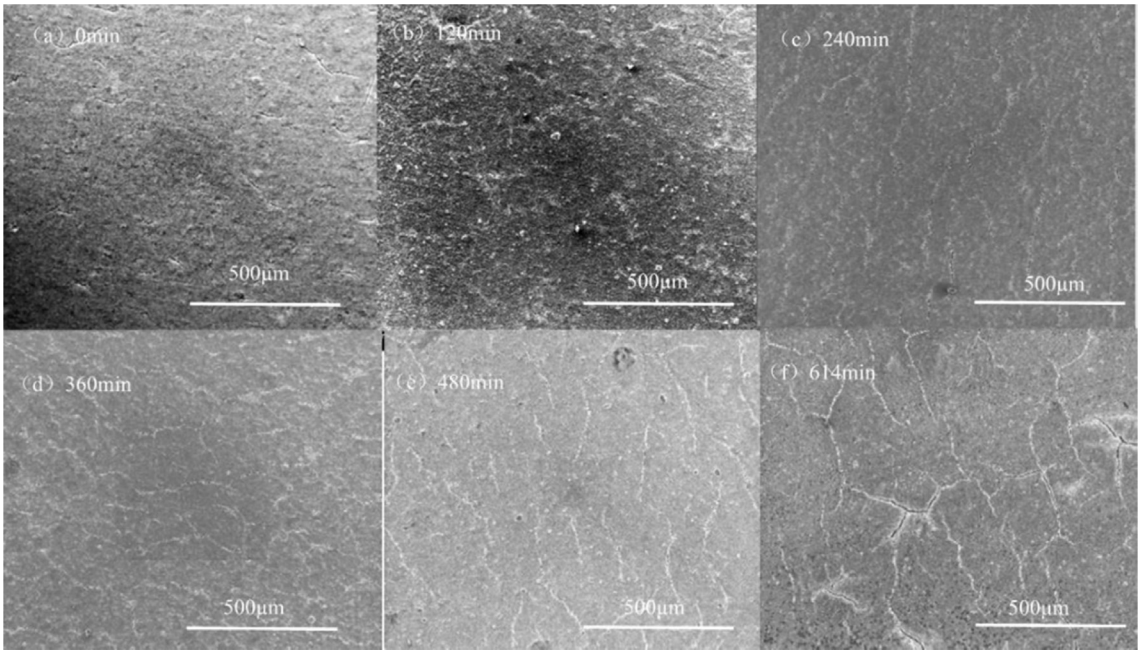


**Fig. 6.** SEM images of the electrode surface in the 2nd cycle of lithiation: (a) SOC0%; (b) SOC10%; (c) SOC20%; (d) SOC30%; delithiation: (e) SOC20%; (f) SOC8.8%.

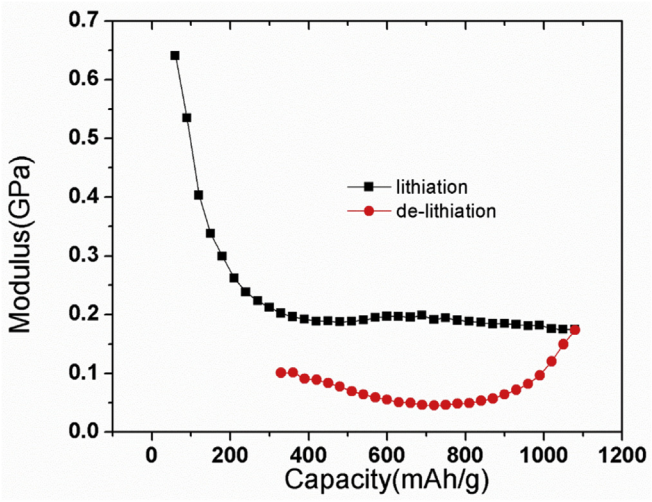


**Fig. 7.** Elastic modulus of the Si composite electrode as a function of the electrode capacity (which is proportional to lithium concentration) during the 2nd cycle.

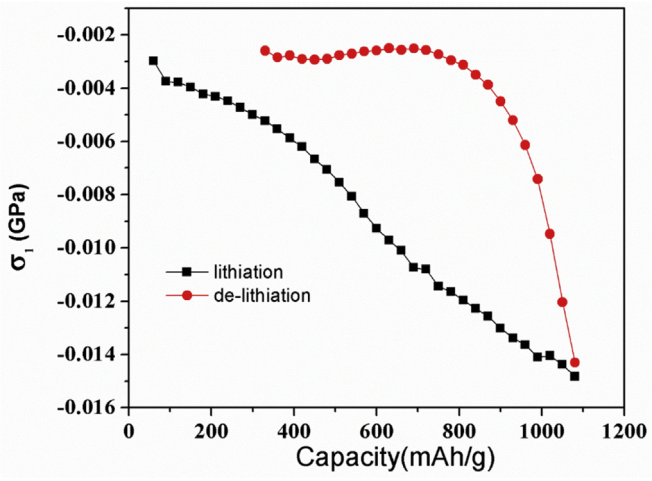


**Fig. 8.** Stress evolution during the 2nd lithiation/delithiation cycle of the composite electrode at C/20 rate.

second lithiation. In the delithiation process, the modulus decreases further with Li extraction, which is opposite to the expected trend of modulus change vs. lithium concentration in $Li_xSi_{1-x}$ [19]. However, this trend can be explained by the formation of cracks. Because stresses on the porous composite electrode exist during both lithiation and delithiation, which may sever the connection between the binder and active particles. Furthermore, more small cracks may form near the pores in the active plate during delithiation [25], which could lead to a further decrease in the modulus of the composite since the active layer containing cracks should have a smaller elastic modulus value than the one without cracks [26]. These cracks are thought to be partially tensile around the pores, although the overall stress is compressive.

The stress can be obtained from Eqs. (2) and (5) and are shown in Fig. 8. During lithiation, the compression increases linearly against the capacity. The resulting compressive stress in the Si/PVDF layer is measured *in situ* to be 0.015 GPa at a capacity of 1080 $mAhg^{-1}$. However, upon delithiation, the stress rapidly becomes less compressive, reducing its absolute value by approximately 82% from its peak value. This large reduction in compressive stress happens during the initial 33% of delithiation, as shown in Fig. 8, due to volume contraction and fracture during delithiation [27], which is consistent with observations shown in Fig. 6. This is similar to the results of CMC/silicon composite electrode, which is measured by a multi-beam optical stress sensor (MOSS) wafer-curvature system [28]. Compared with the MOSS system, our device is simpler more economical, consisting of a CCD camera and a home-made quartz cell. By considering large deformation, our device can measure elastic modulus, as well as stress, while a MOSS device is typically used to measure stress using Stoney equation. Unlike most nanoindentation [29] and micro tensile [30] tests, our

device can perform *in situ* measurements of the mechanical properties and stress evolution in an electrochemical environment.

## 4. Conclusion

An *in situ* method to measure the curvature, elastic modulus and stress evolution in the composite Si/PVDF electrode is reported. A cantilever Si composite electrode structure and a quartz cell were designed and built for the *in situ* measurements. A mathematical model was established for analyzing the relationship between the elastic modulus, in-plane strain, stress evolution, and curvature. The results show that the modulus drops substantially from ca.0.64 GPa to ca. 0.18 GPa in the lithiation process. The modulus decreases further in the delithiation process due to the formation of cracks. The magnitude of compressive stress increases from 0.003 GPa to 0.015 GPa in the lithiation process, and decreases rapidly in the initial delithiation process, which is caused by the volume contraction and crack formation.

## Acknowledgement

The authors gratefully acknowledge the financial supports of the National Science Foundation of China under Grant No. 11332005 and 11172159, and the Shanghai Municipal Education Commission, China, under Grant No. 13ZZ070. Dawei Li would like to acknowledge the support of China Scholarship Council. Yikai Wang, Jiazhi Hu, and Y.-T. Cheng would like to acknowledge the support from US National Science Foundation Award 1355438 (Powering the Kentucky Bioeconomy for a Sustainable Future).

## Appendix

*Volume fraction of each component in the composite electrode*

Our electrode is typically a rectangular shape with length 1.5 *cm* and width 0.3 *cm* and 12 μm in thickness. The average mass is 7.714 mg, and the copper foil is 7 mg. Therefore, the mass of the composite (m) is 0.714 mg. The volume of the electrode can be calculated as $V_{\text{actual}} = \text{L}\times\text{W}\times\text{h} = 1.5\times0.3\times0.0012 = 0.00054\ \text{cm}^3$.

According to the relation of mass, density and volume, the volume fraction of each component is:

$$\Phi_i = \frac{V_i}{V_{actual}} \times 100\% = \frac{M_i}{\rho_i \times V_{actual}} \times 100\% \quad \text{(A1)}$$

Porosity of the composite electrode can be extracted as:

$$Porosity = \frac{V_{actual} - V_{Si} - V_{CB} - V_{PVDF}}{V_{actual}} \times 100\% \quad \text{(A2)}$$

where, $V$ is the volume of the composition in electrode including silicon, carbon black, binder and porosity, ρ is the density. The calculated volume fractions are given in the following table.

## References

[1] J. Christensen, J. Newman, Stress generation and fracture in lithium insertion materials, J. Solid State Electrochem. 10 (2006) 293–319.
[2] Y.T. Cheng, M.W. Verbrugge, Evolution of stress within a spherical insertion electrode particle under potentiostatic and galvanostatic operation, J. Power Sources 190 (2009) 453–460.
[3] J. Zhang, B. Lu, Y. Song, X. Ji, Diffusion induced stress in layered Li-ion battery electrode plates, J. Power Sources 209 (2012) 220–227.
[4] W.J. Zhang, A review of the electrochemical performance of alloy anodes for lithium-ion batteries, J. Power Sources. 196 (2011) 13–24.
[5] X.H. Liu, J.Y. Huang, In situ TEM electrochemistry of anode materials in lithium ion batteries, Energy Environ. Sci. 4 (2011) 3844–3860.
[6] S.C. Chao, Y.C. Yen, Y.F. Song, Y.M. Chen, H.C. Wu, N.L. Wu, A study on the interior microstructures of working Sn particle electrode of Li-ion batteries by in situ X-ray transmission microscopy, Electrochem. Commun. 12 (2010) 234–237.
[7] D. Aurbach, M. Koltypin, H. Teller, In situ AFM imaging of surface phenomena on composite graphite electrodes during lithium insertion, Langmuir 18 (2002) 9000–9009.
[8] L.Y. Beaulieu, T.D. Hatchard, A. Bonakdarpour, M.D. Fleischauer, J.R. Dahn, Reaction of Li with alloy thin films studied by in Situ AFM, J. Electrochem Soc. 150 (2003) A1457–A1464.
[9] B. Key, R. Bhattacharyya, M. Morcrette, V. Seznec, J.M. Tarascon, C.P. Grey, Real-time NMR investigations of structural changes in silicon electrodes for lithium-ion batteries, J. Am. Chem. Soc. 131 (2009) 9239–9249.
[10] Y. Tian, A. Timmons, J.R. Dahn, In situ AFM measurements of the expansion of nanostructured Sn–Co–C films reacting with lithium, J. Electrochem Soc. 156 (2009) A187–A191.
[11] L.Y. Beaulieu, K.W. Eberman, R.L. Turner, L.J. Krause, J.R. Dahn, Colossal reversible volume changes in lithium alloys, Electrochem Solid-State Lett. 4 (2001) A137–A140.
[12] A. Mukhopadhyay, A. Tokranov, K. Sena, X. Xiao, B.W. Sheldon, Thin film graphite electrodes with low stress generation during Li-intercalation, Carbon 49 (2011) 2742–2749.
[13] V.A. Sethuraman, M.J. Chon, M. Shimshak, V. Srinivasan, P.R. Guduru, In situ measurements of stress evolution in silicon thin films during electrochemical lithiation and delithiation, J. Power Sources 195 (2010) 5062–5066.
[14] V.A. Sethuraman, V. Srinivasan, A.F. Bower, P.R. Guduru, In situ measurements of stress-potential coupling in lithiated silicon, J. Electrochem Soc. 157 (2010) A1253–A1261.
[15] V.A. Sethuraman, M.J. Chon, M. Shimshak, V. Srinivasan, P.R. Guduru, In situ measurement of biaxial modulus of Si anode for Li-ion batteries, Electrochem Commun. 12 (2010) 1614–1617.
[16] S.K. Soni, B.W. Sheldon, X. Xiao, A. Tokranov, Thickness effects on the lithiation of amorphous silicon thin films, Scr. Mater 64 (2011) 307–310.
[17] G.G. Stoney, The tension of metallic films deposited by electrolysis, Proc. R. Soc. (Lond) A 82 (1909) 172–175.
[18] Y. Qi, H. Guo, L.G. Hector, A. Timmons, Threefold increase in the Young's modulus of graphite negative electrode during lithium intercalation, J. Electrochem Soc. 157 (2010) A558–A566.
[19] B. Yang, Y.P. He, J. Irsa, C.A. Lundgren, J.B. Ratchford, Y.P. Zhao, Effects of composition-dependent modulus, finite concentration and boundary constraint on Li-ion diffusion and stresses in a bilayer Cu-coated Si nanoanode, J. Power Sources 204 (2012) 168–176.
[20] J. Xu, Q. Zhang, Y.T. Cheng, High capacity silicon electrodes with nafion as binders for lithium-ion batteries, J. Electrochem Soc. 163 (2016) A401–A405.
[21] D. Li, Z. Li, Y. Song, J. Zhang, Analysis of diffusion induced elastoplastic bending of bilayer lithium-ion battery electrodes, Appl. Math. Mech.-Engl.Ed. 37 (2016) 659–670.
[22] X. Liu, D. Chao, Q. Zhang, H. Liu, H. Hu, J. Zhao, Y. Li, Y. Huang, J. Lin, Z.X. Shen, The roles of lithium-philic giant nitrogen-doped graphene in protecting micron-sized silicon anode from fading, Sci. REP-UK (2015) 5.
[23] Y. Song, X. Shao, Z. Guo, J. Zhang, Role of material properties and mechanical constraint on stress-assisted diffusion in plate electrodes of lithium ion batteries, J. Phys. D. Appl. Phys. 10 (2013) 105307.
[24] D.R. Frear, S.N. Burchett, H.S. Morgan, J.H. Lau (Eds.), The Mechanics of Solder Alloy Interconnects, Van Nostrand Reinhold, New York, 1994.
[25] C.G. Sammis, M.F. Ashby, The failure of brittle porous solids under compressive stress states, Acta Metall. 34 (1986) 511–526.
[26] X. Zhang, M. Watanabe, S. Kuroda, Effects of residual stress on the mechanical properties of plasma-sprayed thermal barrier coatings, Eng. Fract. Mech. 110 (2013) 314–327.
[27] S.K. Soni, B.W. Sheldon, X. Xiao, M.W. Verbrugge, A. Dongjoon, H. Haftbaradaran, G. Huajian, Stress mitigation during the lithiation of patterned amorphous Si islands, J. Electrochem Soc. 1 (2011) A38–A43.
[28] V.A. Sethuraman, A. Nguyen, M.J. Chon, S.P. Nadimpalli, H. Wang, D.P. Abraham, A.F. Bower, V.B. Shenoy, P.R. Guduru, Stress evolution in composite silicon electrodes during lithiation/delithiation, J. Electrochem Soc. 4 (2013) A739–A746.
[29] B. Hertzberg, J. Benson, G. Yushin, Ex-situ depth-sensing indentation measurements of electrochemically produced Si–Li alloy films, Electrochem. Commun. 13 (8) (2011) 818–821.
[30] R. Liu, H. Wang, X. Li, G. Ding, C. Yang, A micro-tensile method for measuring mechanical properties of MEMS materials, J. Micromech Microeng 18 (6) (2008) 065002.